Journal of Power Sources 257 (2014) 198–204

Contents lists available at ScienceDirect

Journal of Power Sources

journal homepage: www.elsevier.com/locate/jpowsour

Hollow $Li_{1.2}Mn_{0.5}Co_{0.25}Ni_{0.05}O_2$ microcube prepared by binary template as a cathode material for lithium ion batteries

S.J. Shi, Z.R. Lou, T.F. Xia, X.L. Wang, C.D. Gu, J.P. Tu*

State Key Laboratory of Silicon Materials, Key Laboratory of Advanced Materials and Applications for Batteries of Zhejiang Province, and Department of Materials Science and Engineering, Zhejiang University, Hangzhou 310027, China

HIGHLIGHTS

- Novel $Li_{1.2}Mn_{0.5}Co_{0.25}Ni_{0.05}O_2$ microcube is prepared through a simple binary template.
- Hollow circle cube architecture is formed.
- High initial discharge capacity of 272.9 mAh g^{-1} can be obtained at 0.1 C.
- Improved rate capability with discharge capacity of 110 mAh g^{-1} is obtained at 10 C.

ARTICLE INFO

Article history:
Received 22 November 2013
Received in revised form
10 January 2014
Accepted 4 February 2014
Available online 13 February 2014

Keywords:
Lithium nickel cobalt manganese oxide
Hollow cube
Binary template
Lithium ion battery

ABSTRACT

Novel $Li_{1.2}Mn_{0.5}Co_{0.25}Ni_{0.05}O_2$ microcube is prepared through a simple binary template method. After calcined at 800 °C, lithium and nickel are permeated into the cathode material and a well-crystallized Li-rich layered oxide is obtained. Furthermore, hollow circle cube architecture is formed due to the decomposing of the carbonate. As a cathode material for lithium ion batteries (LIBs), the oxide with such architecture can deliver high initial discharge capacity of 272.9 mAh g^{-1} at a current density of 20 mA g^{-1}. High reversible discharge capacities of 208 mAh g^{-1} and 110 mAh g^{-1} are obtained at a current density of 200 mA g^{-1} and 2000 mA g^{-1}, respectively. Cyclic voltammetry (CV) and electrochemical impedance spectroscopy (EIS) are performed to further study the hollow $Li_{1.2}Mn_{0.5}Co_{0.25}Ni_{0.05}O_2$ microcube. It is remarkable that such architecture makes the Li-rich layered oxide $Li_{1.2}Mn_{0.5}Co_{0.25}Ni_{0.05}O_2$ a promising cathode material for LIBs.

1. Introduction

Over the last decade, lithium ion batteries (LIBs) have developed rapidly due to the exhaustion of fossil fuels and the urgent need for environment problems. Cathode material is considered as the key part of LIBs and has be widely investigated, from the early $LiCoO_2$ [1] to nowadays $LiFePO_4$ [2,3], $LiMn_2O_4$ [4], $LiMn_xNi_yCo_{1-x-y}O_2$ [5–7] and Li-rich compounds [8–21]. Among them, it is attractive that the Li-rich compounds such as $Li_{1.2}Mn_{0.54}Ni_{0.13}Ni_{0.13}O_2$ can deliver higher discharge capacity over 250 mAh g^{-1} [10,13] than those belonging to other cathode systems after activation in the initial cycle. However, due to the complex components of such cathode material and lack of controllable technique, large particles with serious agglomeration are always obtained via traditional solid state reactions, resulting in poor electrochemical performances especially at high current densities [22]. The high performance LIBs application of Li-rich compounds is thus limited to a great extent.

The controllable construction of the material morphology has been considered as one of the most efficient way to improve the electrochemical performances. Recently, various structured electrode materials, such as nanorods or tubes [23–27], nanosheets or plates [28,29], hollow or core–shell spheres [30–33], ordered/disordered mesoporous/macroporous materials [34,35] and three dimensional (3D) network architectures [36–38] have been fabricated via various methods to improve the electrochemical performances. In particular, hollow micro/nanostructures with well-formed morphology and composition have attracted lots of attentions in recent years [31–33,39–41]. Generally, the electrode materials with hollow architectures may contribute a lot to the improved electrochemical performances. The hole in each hollow particle may provide lots of extra active sites as the storage of Li^+, resulting in enhancing the electrochemical kinetics. Furthermore,

* Corresponding author. Tel.: +86 571 87952856; fax: +86 571 87952573.
E-mail addresses: tujp@zju.edu.cn, tujplab@zju.edu.cn (J.P. Tu).

http://dx.doi.org/10.1016/j.jpowsour.2014.02.011
0378-7753/

the hollow structure often enlarges the specific surface area and reduces effective diffusion distance for Li^+, leading to an improved electrochemical performance [32].

However, it is difficult to construct controllable morphology of the Li-rich layered compounds due to the complex components including lithium, cobalt, nickel and manganese. It is almost impossible to obtain the compounds (including its precursor) with special architecture naturally or in some stable conditions without any adjustments. It is difficult to get compounds with an atomic mixture level containing all the three elements (Co, Mn, Ni) due to the differences among them. In addition, high temperature solid state reactions which may destroy the architecture of the precursors are usually necessary to form well structured Li-rich compounds. Recently, some research groups use manganese oxides as templates to synthesize lithium manganese nickel oxides or $LiMn_2O_4$ cathode materials [32,42–44]. However, such method is usually performed to synthesize binary Li-rich compounds. It is hard to permeate two different elements (usually Ni and Co) together with large ratio of component to form well formed ternary Li-rich compounds based on manganese oxide templates. We propose a novel binary template method to get ternary Li-rich compounds with only one element to be permeated into. It is facile to get evenly distributed ternary Li-rich compounds without destruction of the architecture. Here, in this present work, hollow novel Li-rich ternary oxide $Li_{1.2}Mn_{0.5}Co_{0.25}Ni_{0.05}O_2$ ($0.5Li_2MnO_3 \cdot 0.5LiMn_{0.25}Co_{0.625}Ni_{0.125}O_2$) microcube is fabricated through such facile binary template strategy followed by high temperature solid state reactions. Such hollow architecture can efficiently improve the electrochemical performances of Li-rich oxide $Li_{1.2}Mn_{0.5}Co_{0.25}Ni_{0.05}O_2$. Although the binary template ($Co_{0.33}Mn_{0.67}CO_3$) performed here has the limitation of component adjustment for the Li-rich compounds (the ratio of Mn and Co is fixed at 2/1), there are many other binary templates can also be used in such strategy to synthesize ternary Li-rich compounds with different components, such as $Li_{1.2}Mn_{0.54}Co_{0.13}Ni_{0.13}O_2$ with attractive architecture. Such strategy exhibits a promising approach to obtain cathode material with specific architecture for high energy lithium ion batteries.

2. Experimental

The binary $Co_{0.33}Mn_{0.67}CO_3$ template with microcube morphology was induced by ammonia evaporation [43]. 1.65 mmol $Co(NO_3)_2 \cdot 6H_2O$, 3.35 mmol $MnSO_4 \cdot H_2O$, 35 mL alcohol and 50 mmol $(NH_4)_2SO_4$ were dissolved in 350 mL de-ionized water as solution A. 50 mmol NH_4HCO_3 was also dissolved in 350 mL de-ionized water as solution B. First, solution A and B were mixed thoroughly. Then, continue stirring was performed at 50 °C for 9 h. With the continue evaporation of the ammonia, the metal ions were deposited by the carbonate to form $Co_{0.33}Mn_{0.67}CO_3$ with microcube morphology. Similar methods [32,43–48] are widely performed to obtain deposition with unique morphology. After that, the deposition was filtrated and washed by de-ionized water and alcohol thoroughly. After drying, the $Co_{0.33}Mn_{0.67}CO_3$ precursor was dispersed together with stoichiometric amounts of $LiOH \cdot H_2O$ and $Ni(NO_3)_2 \cdot 6H_2O$ in alcohol. The suspension was then heated to 50 °C and evaporated until dryness. At last, the mixture was ground manually for 1 h, heated at 800 °C for 16 h in air to obtain final $Li_{1.2}Mn_{0.5}Co_{0.25}Ni_{0.05}O_2$.

As a comparison, Li-rich compound with the same component is also synthesized by traditional sol–gel processes. Stoichiometric amounts of $LiCH_3COO \cdot 2H_2O$, $Ni(CH_3COO)_2 \cdot 4H_2O$, $Co(CH_3COO)_2 \cdot 4H_2O$, $Mn(CH_3COO)_2 \cdot 4H_2O$ were dissolved in de-ionized water with citric acid as the chelating agent to get a transparent solution. Then, the resulting solution was heated to 80 °C and stirred to remove the water slowly till a transparent sol and then gel was formed. The gel was calcined at 800 °C for 16 h in air to get the final $Li_{1.2}Mn_{0.5}Co_{0.25}Ni_{0.05}O_2$. The as-synthesized oxides were named as T-LMNCO and SG-LMNCO for those synthesized by binary template and sol–gel method for short, respectively.

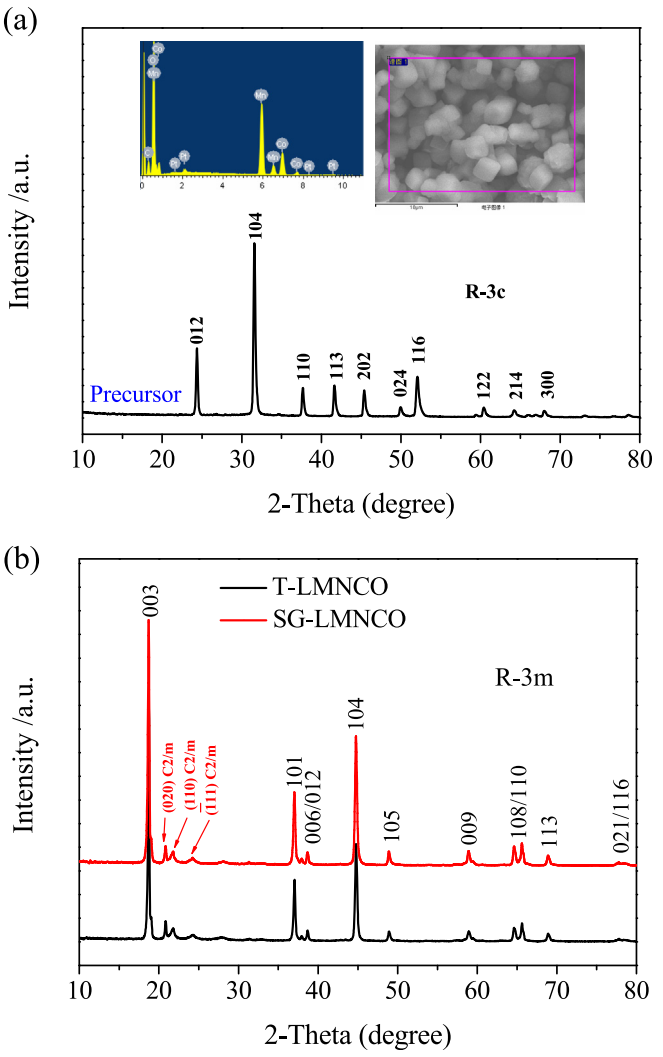

Fig. 1. XRD patterns of (a) $Co_{0.33}Mn_{0.67}CO_3$ precursor and (b) $Li_{1.2}Mn_{0.5}Co_{0.25}Ni_{0.05}O_2$ powders synthesized by binary template and sol–gel. The inset in (a) is the result of the EDAX for the $Co_{0.33}Mn_{0.67}CO_3$ precursor.

The structures and morphologies of the as-prepared powders were characterized by field emission scanning electron microscopy (Hitachi SU-70 coupled with EDX) and high-resolution transmission electron microscopy (TEM, Tecnai G2 F30 S-Twin). XRD measurements were collected using CuKα radiation at 250 mA and 40 kV from 10.0° to 80.0°, with an increasing step size of 0.02°, counting time duration of 1.0 s for each step on a Rigaku D/Max-2550pc X-Ray diffractometer. The specific surface areas of the powders were measured following the multipoint Brunauer–Emmett–Teller (BET) procedure from the N_2 adsorption/desorption isotherms using an AUTOSORB-1-C gas sorption analyzer.

A slurry coating procedure was performed to prepare the working electrodes. The slurry consisted of 85 wt.% active materials, 10 wt.% carbon conductive agent (acetylene black) and 5 wt.% polyvinylidene fluoride (PVDF) were coated uniformly on treated aluminum foil. After drying at 90 °C in vacuum for 24 h, the aluminum foil with active material was pressed under a pressure of

20 MPa. 1 M $LiPF_6$ in ethylene carbonate (EC)–dimethyl carbonate (DMC) (1:1 in volume) was used as the electrolyte and a metallic lithium foil served as the anode, a polypropylene micro-porous film (Cellgard 2300) as the separator. Finally, the cells with coin-type cells (CR2025) were assembled in an argon-filled glove box with H_2O concentration below 1 ppm. The galvanostatic discharge–charge tests were performed on a LAND battery program-control test system (Wuhan, China) between 2.0 and 4.8 V at current densities from 20 mA g^{-1} to 2000 mA g^{-1} at room temperature. Cyclic voltammetry (CV) tests were carried out on an electrochemical workstation (CHI660C) in the potential window of 2.0–5.0 V (vs. Li/Li^+) at a scan rate of 0.1 mV s^{-1}. Electrochemical impedance spectroscopy (EIS) measurements were performed on the same apparatus using a three-electrode cell with the Li-rich compounds as the working electrode, metallic lithium foil as both the counter and reference electrodes. The amplitude of the AC signal was 5 mV over a frequency range from 100 kHz to 10 MHz at the charge state of 4.5 V.

3. Results and discussion

3.1. Material characterization

The XRD patterns of the cube $Co_{0.33}Mn_{0.67}CO_3$ precursor and the final Li-rich $Li_{1.2}Mn_{0.5}Co_{0.25}Ni_{0.05}O_2$ layered oxide are shown in Fig. 1. After filtering and drying, all the diffraction peaks of the precursor reflect a similar lattice character as rhombohedral phase of $MnCO_3$ which belongs to the space group of R-3c, based on the hexagonal structure [45,46]. No distinct impurity is observed from Fig. 1a, indicating high purity of the $Co_{0.33}Mn_{0.67}CO_3$ precursor. In addition, EDAX test is performed to show the approximate atomic proportion of Mn and Co, as shown in the inset of Fig. 1a. The calculated value of Mn/Co is approaching to 2. The results of XRD and EDAX indicate that $Co_{0.33}Mn_{0.67}CO_3$ precursor is obtained with the right component and structure.

Fig. 1b shows the XRD patterns of the Li-rich layered oxides T-LMNCO and SG-LMNCO. All the diffraction peaks of both the oxides can be indexed on the basis of the α-$NaFeO_2$ structure with space group R-3m without any impurity, except for the super lattice peaks between 20° and 30°. Distinct splitting (006)/(102) and (108)/(110) peaks can be observed, which indicate well-formed layered structure [7,49]. The weak peaks between 20° and 30° for the Li-rich layered oxides can be indexed to the monoclinic unit cell C2/m [50,51]. They are consistent with the $LiMn_6$ cation arrangement that occurs in the transition metal layers of Li_2MnO_3 region or nano-domains. For both synthesis methods, pure Li-rich layered oxides $Li_{1.2}Mn_{0.5}Co_{0.25}Ni_{0.05}O_2$ are obtained.

Fig. 2a and b shows the SEM images of the cube $Co_{0.33}Mn_{0.67}CO_3$ precursors at low and high magnifications, respectively. The cube precursor particles with sizes of about 3–5 μm are solid without any hollow pore in the particle center. At high magnification in Fig. 2b, it is observed that the cube is composed of numerous nanoparticles, which form relatively smooth surface. Fig. 2c shows the final product after calcined at 800 °C. It is obvious that the cube

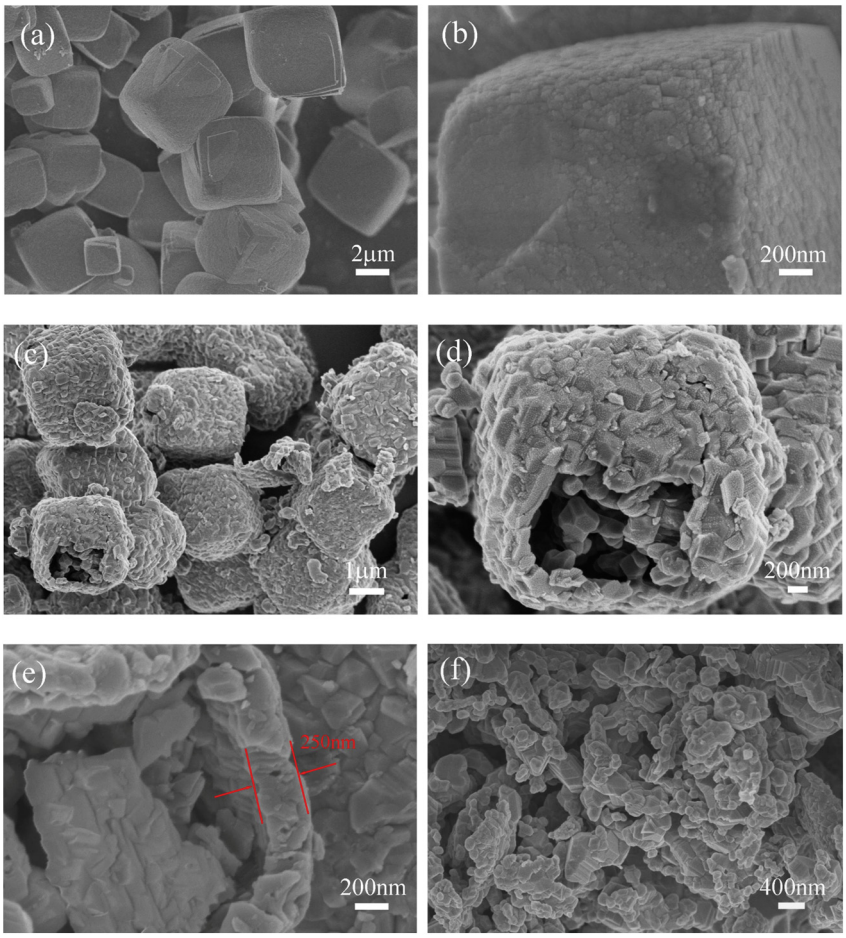

Fig. 2. SEM images of (a), (b) $Co_{0.33}Mn_{0.67}CO_3$ precursor and (c), (d), (e) $Li_{1.2}Mn_{0.5}Co_{0.25}Ni_{0.05}O_2$ powder prepared by binary template method at different magnifications, (f) $Li_{1.2}Mn_{0.5}Co_{0.25}Ni_{0.05}O_2$ powder prepared by sol–gel method.

morphology is retained after the addition of Li, Ni source and high temperature solid state reactions. However, from Fig. 2d, it can be found that the cubes become hollow. It is attributed to the thermal decomposition of the carbonate during the high temperature reactions. There is not only the decomposition of the carbonate, but also the crystal or particle growth. The heating and the high temperature reactions are also non-equilibrium in microcosm. It seems that in order to reach the state with the lowest energy, the crystal will grow larger and the small pores may also tend to get together forming a large hole to reduce the surface energy. So the carbon dioxide was removed from the cube structure, leaving hollow center with some remained particles in the cavity. Simultaneously, the primary particles become much larger with sizes of 200–400 nm due to the high temperature calcination. The surface of the cube oxide thus becomes rougher in contrast to the $Co_{0.33}Mn_{0.67}CO_3$ precursor. The thickness of the shell is about 250 nm which is approximately equivalent to the size of the primary particles, as shown in Fig. 2e. Fig. 2f shows the SEM image of the Li-rich layered oxide $Li_{1.2}Mn_{0.5}Co_{0.25}Ni_{0.05}O_2$ synthesized by sol–gel method. A normal morphology with large agglomeration composing of primary particles (200–500 nm) is observed after calcined at 800 °C. No special architecture is achieved without any template through sol–gel method. The hollow cube architecture of T-LMNCO can also be observed clearly through TEM images (Fig. 3a). Dark shell with a thickness of 200–400 nm encircles the bright cavity in the center. Furthermore, the remained primary particles form a dark core, which make the bright cavity become a bright ring. It is accordant with the results observed from the SEM images. The HRTEM image demonstrates that the distance of 0.467 nm not only agrees well with the {003} lattice spacing of the rhombohedral phase of lithium nickel manganese cobalt oxide, but also the {001} planes for monoclinic Li_2MnO_3 (Fig. 3b), indicating the formation of high crystalline oxide.

Nitrogen adsorption/desorption isotherms recorded for the $Li_{1.2}Mn_{0.5}Co_{0.25}Ni_{0.05}O_2$ powders synthesized by sol–gel and binary template methods are shown in Fig. 4. The Brunauer, Emmett, and Teller surface area values obtained from the adsorption isotherms in the p/p_0 range below 0.30 are 3.215 $m^2\ g^{-1}$ and 5.084 $m^2\ g^{-1}$ for SG-LMNCO and T-LMNCO, respectively. The BET area of T-LMNCO is larger than that of SG-LMNCO which can be ascribed to the special architecture. The total pore volume of T-LMNCO is 4.496×10^{-2} $cm^3\ g^{-1}$, much larger than that of SG-LMNCO, 1.775×10^{-2} $cm^3\ g^{-1}$, which is also attributed to the formation of the hollow structure.

3.2. Electrochemical properties

The electrochemical performances of the $Li_{1.2}Mn_{0.5}Co_{0.25}Ni_{0.05}O_2$ with hollow cube structure are performed to compare with those of SG-LMNCO. As shown in Fig. 5a, the initial charge–discharge curves of T-LMNCO at a current density of 20 mA g^{-1} in the voltage range of 2.0–4.8 V at room temperature, depict a high initial discharge capacity of 272.9 mAh g^{-1} with a coulombic efficiency of 75.2%. The low initial coulombic efficiency here can be explained as follows: As normal Li-rich layered oxides, the charge processes are extremely complex. Simply, the initial charge process can be divided into two parts, one from 3.8 V to 4.4 V and the other at about 4.5 V. The first part is considered as a reversible process including the Li-extraction from the structure of space group R-3m accompanying with the oxidation of mainly Ni^{2+}/Ni^{4+} and partly Co^{3+}/Co^{4+}. The other at about 4.5 V is irreversible but very important which represents the activation of the Li_2MnO_3-like region appearing only in the initial cycle [52,53]. Thus, Li ions extracted from Li_2MnO_3-like region cannot be re-inserted into the new formed structure, resulting in the low initial coulomb efficiency [52,53]. The charge capacities of both the electrodes approach to the theoretical value (376.3 mAh g^{-1}, calculated from the parent $Li[Li_{0.2}Mn_{0.50}Ni_{0.05}Co_{0.25}]O_2$), 363.0 mAh g^{-1} and 345.7 mAh g^{-1} for T-LMNCO and SG-LMNCO, respectively. And after the initial activation, it seems that "1 Li^+" can be re-inserted into the newly formed layered structure. Initial discharge capacities of

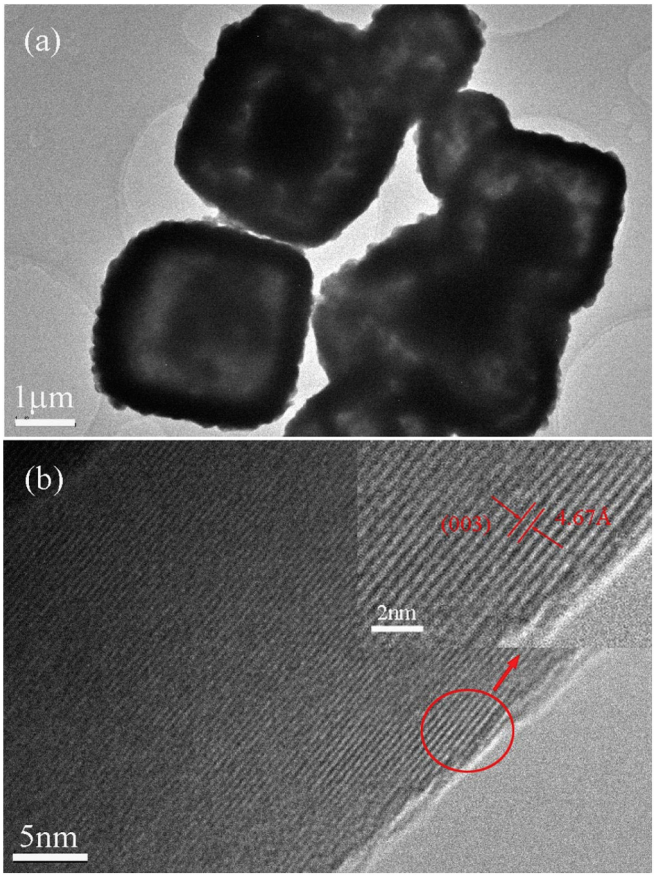

Fig. 3. TEM images of $Li_{1.2}Mn_{0.5}Co_{0.25}Ni_{0.05}O_2$ powder synthesized by the binary template method. The inset in (b) is the magnification of the red cycle in (b). (For interpretation of the references to color in this figure legend, the reader is referred to the web version of this article.)

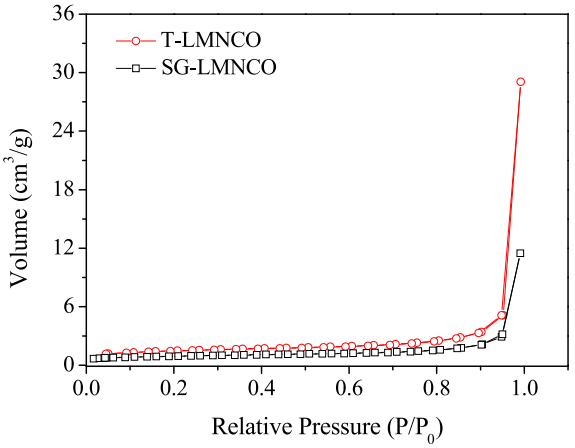

Fig. 4. Nitrogen adsorption–desorption isotherms of $Li_{1.2}Mn_{0.5}Co_{0.25}Ni_{0.05}O_2$ powders synthesized by binary template and sol–gel method.

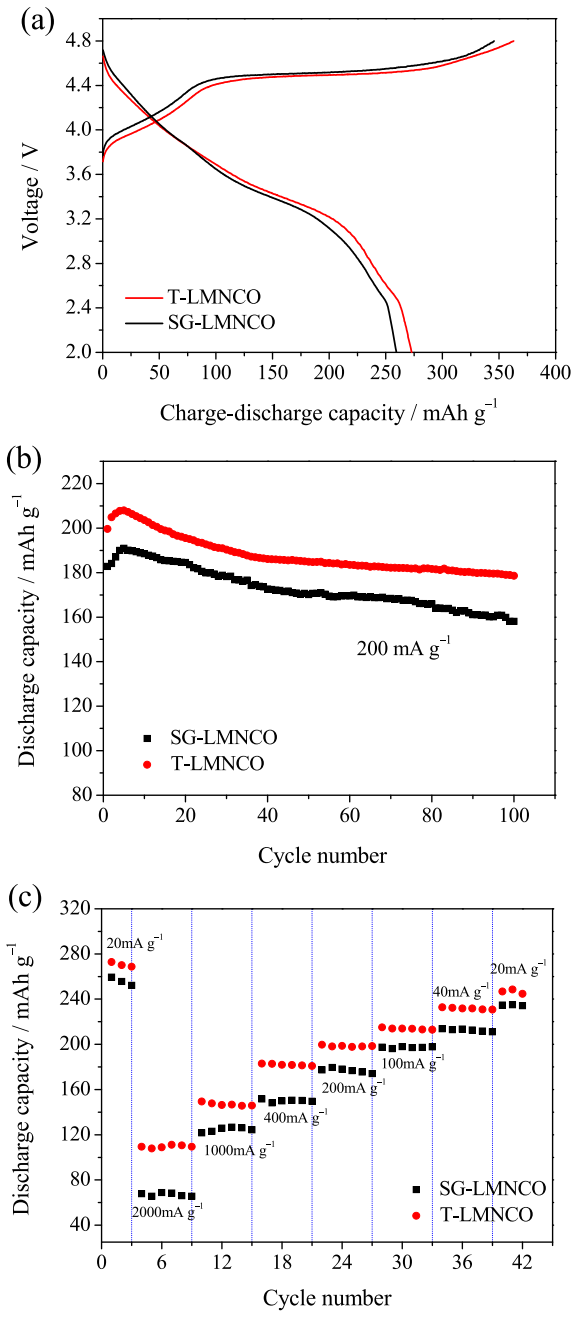

Fig. 5. (a) Initial charge–discharge curves of $Li_{1.2}Mn_{0.5}Co_{0.25}Ni_{0.05}O_2$ synthesized by binary template and sol–gel method at a current density of 20 mA g^{-1} in the voltage range of 2.0–4.8 V; (b) Cycle performances of $Li_{1.2}Mn_{0.5}Co_{0.25}Ni_{0.05}O_2$ electrodes at a current density of 200 mA g^{-1}; (c) Rate capability of $Li_{1.2}Mn_{0.5}Co_{0.25}Ni_{0.05}O_2$ electrodes, the cell is charged and discharged at the same current densities.

272.9 mAh g^{-1} and 259.4 mAh g^{-1} are obtained, which approach to the theoretical value of 281.0 mAh g^{-1} (calculated from the newly formed layered oxide $Mn_{0.625}Co_{0.3125}Ni_{0.0625}O_2$). T-LMNCO with hollow cube structure has higher initial discharge capacity than that of SG-LMNCO. When the current density increases to 200 mA g^{-1}, the initial discharge capacity is 199.6 mAh g^{-1} for T-LMNCO and the discharge capacity reaches the maximum (208.0 mAh g^{-1}) after several cycles. It is higher than that of SG-LMNCO, 190.9 mAh g^{-1} as the maximum obtained after several cycles. In addition, both T-LMNCO and SG-LMNCO electrodes have good cyclic stability, about 178.6 mAh g^{-1} and 158.1 mAh g^{-1} with capacity retention of 85.87% and 82.82% are obtained after 100 cycles at 200 mA g^{-1}, respectively (Fig. 5b). The reasons for the decline of the capacity during cycling can be ascribed to Jahn-Teller distortion, as well as the side reactions between the active materials and electrolyte which result in the dissolution of the metal ions [8,53–57]. A lot of approaches have been proposed to improve the cycling stability of the Li-rich compounds, such as surface modification [8], graphitic nanofibers adding [12], the improving of the interfacial stability [58,59] and so on. As shown in Fig. 5c, with increasing the discharge current densities from 20 mA g^{-1} to 2000 mA g^{-1}, the specific discharge capacities of T-LMNCO are much higher than those of SG-LMNCO. Up to 2000 mA g^{-1}, T-LMNCO can still deliver a discharge capacity of about 110 mAh g^{-1}. However, only about 68 mAh g^{-1} is left for SG-LMNCO. The reversible capacity of the Li-rich layered oxide at high current density is enhanced when the hollow microcube is introduced. It makes the hollow Li-rich layered oxide microcube a promising cathode material for high-performance LIBs.

In order to further study the hollow $Li[Li_{0.2}Mn_{0.50}Ni_{0.05}Co_{0.25}]O_2$ microcube cathode material, CV tests were performed to further understand the effect of such unique architecture. The initial three CV curves of SG-LMNCO and T-LMNCO are shown in Fig. 6a and b. The initial CV curves for both the electrodes are sharp and symmetrical. There are two main anodic peaks in the initial cycle. One is at about 4.0 V and the other is at about 4.6 V (vs. Li/Li$^+$). The one at about 4.0 V is ascribed to the Li^+ extraction from the $LiMO_2$ (M = Mn, Ni, Co) structure accompanying with the oxidation of the Ni^{2+}/Ni^{4+} and Co^{2+}/Co^{4+}, corresponding to the first platform of the

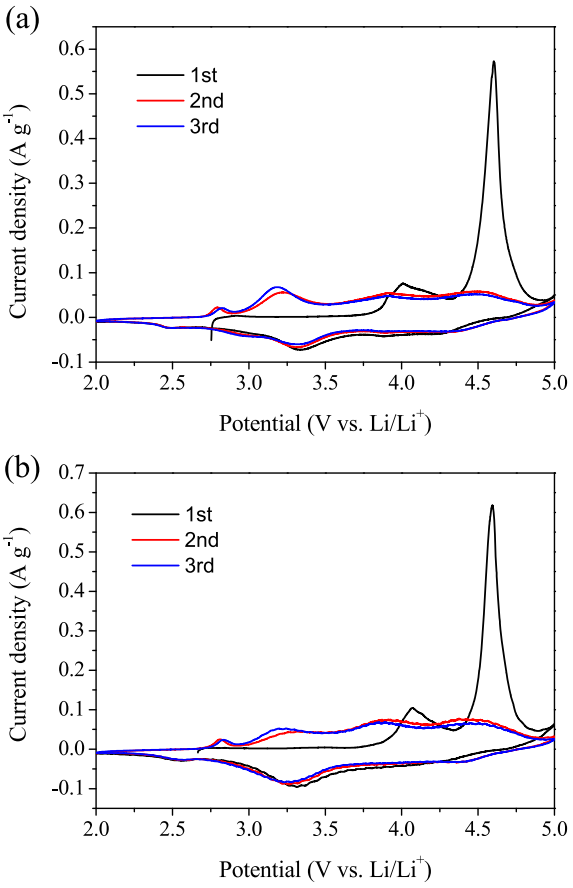

Fig. 6. CV curves of $Li_{1.2}Mn_{0.5}Co_{0.25}Ni_{0.05}O_2$ powders synthesized by (a) binary template and (b) sol–gel method for the initial three cycles in the potential range of 2.0–5.0 V (vs. Li/Li$^+$) at a scan rate of 0.1 mV s^{-1}.

initial charge–discharge curve. And the other peak at 4.6 V is associated with the activation of the Li_2MnO_3 region, extraction of Li^+ from $Li[Li_{1/3}Mn_{2/3}]O_2$, corresponding to the second platform. After activation, the inactive $Li[Li_{1/3}Mn_{2/3}]O_2$ amazingly becomes electrochemical active $[MO_2]$. During the following discharge process, high initial discharge capacity can be obtained for both the electrodes due to the newly formed layered oxides $[MO_2]$. However, in the second cycle, the activation peak disappears. A small peak at about 2.8 V and three large peaks at about 3.2 V, 3.85 V, 4.4 V appear, which are the main anodic peaks for the newly formed [M]O_2 (M = Mn, Ni, Co). During the reduction process, a small cathodic peak at about 2.5 V and two large cathodic peaks at about 3.25 V, 4.25 V are evident. Because of the complex component and reactions, it is impossible to differentiate the reduction and oxidation processes of the individual Mn, Ni and Co from the data [60]. Although both the electrodes have similar CV curves, the current density of T-LMNCO is obviously stronger than that of SG-LMNCO which indicates better electrochemical performances. These results are accordant with the electrochemical performances obtained former.

Before EIS tests were performed, the cells were first charge-discharged for 5 cycles at a current density of 200 mA g^{-1}, and then charged to 4.5 V at a low current density of 20 mA g^{-1}. Fig. 7a and b shows the Nyquist plots of the Li-rich layered oxides SG-LMNCO and T-LMNCO. The shapes of both the Nyquist plots are similar. They are composed of a small interrupt and a semicircle in the high frequency, a semicircle in the high to medium frequency and a quasi-straight line in the low frequency. The small interrupt in the high frequency which corresponds to the solution impedance, is almost the same for both the oxide electrodes. The small semicircle in the high frequency is assigned to the impedance of Li^+ diffusion in the surface layer (R_e); another semicircle in the high to medium frequency indicates the charge transfer impedance (R_{ct}), relating to charge transfer through the electrode/electrolyte interface. And the quasi-straight line in the low frequency represents the Warburg impedance, which is related to the solid-state diffusion of Li^+ in the electrode materials [61,62]. It is obvious that when the electrodes tend to stability after several cycles, the impedance of the T-LMNCO electrode is much smaller than that of the SG-LMNCO, both the R_e and R_{ct}. It seems that the formation of hollow cube architecture can reduce the impedance of the electrode, which may be attributed to the enlarged surface area and the reduced effective Li^+ diffusion length, thus improving the reversible capacity at high current density.

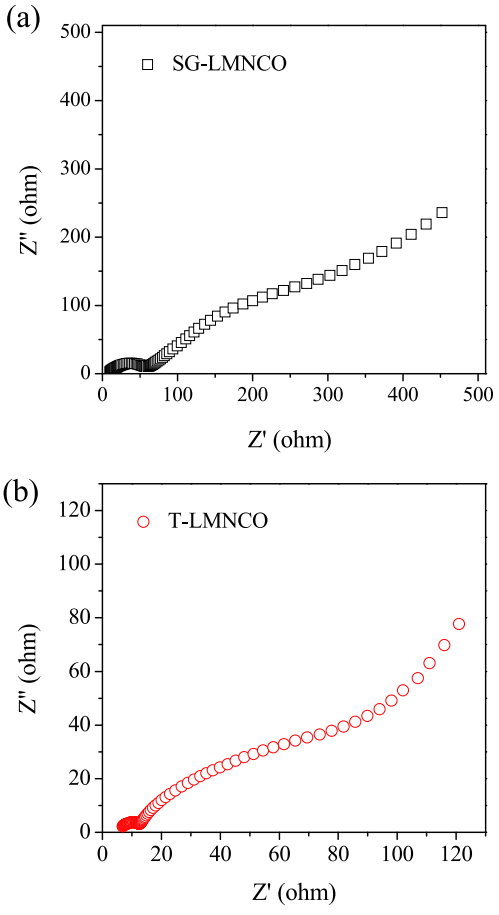

Fig. 7. Nyquist plots of $Li_{1.2}Mn_{0.5}Co_{0.25}Ni_{0.05}O_2$ powders synthesized by (a) binary template, (b) sol–gel method after 5 cycles at the charge state of 4.5 V.

4. Conclusions

Novel hollow $Li_{1.2}Mn_{0.5}Co_{0.25}Ni_{0.05}O_2$ microcube is synthesized via a simple binary template method. Li and Ni are permeated into the structure of the oxide during high-temperature solid state reactions to obtain well-formed layered structure and retain the cube morphology of the precursor. The $Li_{1.2}Mn_{0.5}Co_{0.25}Ni_{0.05}O_2$ with such architecture can deliver high initial discharge capacity with good capacity retention. In addition, an enhanced reversible capacity at high current density is obtained due to the enlarged specific surface area and the reduced Li^+ diffusion distance. Such binary template strategy exhibits a promising approach to obtain cathode material with specific architecture for high energy LIBs.

Acknowledgments

This work is supported by the National Science and Technology Support Program (2012BAC08B08, 2012BAK30B04), the Program for Innovative Research Team in University of Ministry of Education of China (IRT13037) and Key Science and Technology Innovation Team of Zhejiang Province (2010R50013).

References

[1] S.H. Choi, J.H. Kim, Y.N. Ko, K.M. Yang, Y.C. Kang, J. Power Sources 244 (2013) 129.
[2] W.L. Liu, J.P. Tu, Y.Q. Qiao, J.P. Zhou, S.J. Shi, X.L. Wang, C.D. Gu, J. Power Sources 196 (2011) 7728.
[3] J.P. Zhou, J.P. Tu, L.J. Cheng, S.J. Shi, Y.Q. Qiao, W.L. Liu, X.L. Wang, C.D. Gu, J. Electrochem. Soc. 158 (2011) A1237.
[4] H.M. Wu, J.P. Tu, Y.F. Yuan, Y. Li, X.B. Zhao, G.S. Cao, Scr. Mater. 52 (2005) 513.
[5] P. Gao, Y.H. Li, H.D. Liu, J. Pinto, X.F. Jiang, G. Yang, J. Electrochem. Soc. 159 (2012) A506.
[6] C. Nithya, R. Thirunakaran, A. Sivashanmugam, G.V.M. Kiruthika, S. Gopukumar, J. Phys. Chem. C. 113 (2009) 17936.
[7] A.M.A. Hashem, A.E. Abdel-Ghany, A.E. Eid, J. Trottier, K. Zaghib, A. Mauger, C.M. Julien, J. Power Sources 196 (2011) 8632.
[8] S.J. Shi, J.P. Tu, Y.J. Mai, Y.Q. Zhang, C.D. Gu, X.L. Wang, Electrochim. Acta 63 (2012) 112.
[9] S.J. Shi, J.P. Tu, Y.Y. Tang, Y.X. Yu, Y.Q. Zhang, X.L. Wang, J. Power Sources 221 (2013) 300.
[10] J. Liu, B.R. Jayan, A. Manthiram, J. Phys. Chem. C. 114 (2010) 9528.
[11] Z. Li, F. Du, X.F. Bie, J. Phys. Chem. C. 114 (2010) 22751.
[12] S.K. Martha, J. Nanda, G.M. Veith, N.J. Dudney, J. Power Sources 199 (2012) 220.
[13] C.J. Jafta, K.I. Ozoemen, M.K. Mathe, W.D. Roos, Electrochim. Acta 85 (2012) 411.
[14] S.-H. Yu, T. Yoon, J.Y. Mun, S. Park, Y.-S. Kang, J.-H. Park, S.M. Oh, Y.-E. Sung, J. Mater. Chem. A 1 (2013) 2833.
[15] P. Röder, N. Baba, H.-D. Wiemhöfer, J. Power Sources 248 (2014) 978.
[16] S.J. Shi, J.P. Tu, Y.Y. Tang, X.Y. Liu, X.Y. Zhao, X.L. Wang, C.D. Gu, J. Power Sources 241 (2013) 186.
[17] O. Toprakci, H.A.K. Toprakci, Y. Li, L.W. Ji, L.G. Xue, H. Lee, S. Zhang, X.W. Zhang, J. Power Sources 241 (2013) 522.

[18] S.J. Shi, J.P. Tu, Y.Y. Tang, Y.Q. Zhang, X.L. Wang, C.D. Gu, J. Power Sources 240 (2013) 140.
[19] Y. Jiang, Z. Yang, W. Luo, X.L. Hu, W.X. Zhang, Y.H. Huang, J. Mater. Chem. 22 (2012) 14964.
[20] J. Wang, B. Qiu, H.L. Cao, Y.G. Xia, Z.P. Liu, J. Power Sources 218 (2012) 128.
[21] L.G. Xue, S. Zhang, S.L. Li, Y. Lu, O. Toprakci, X. Xia, C. Chen, Y. Hu, X.W. Zhang, J. Alloys Compd. 577 (2013) 560.
[22] J.M. Zheng, X.B. Wu, Y. Yang, Electrochim. Acta 56 (2011) 3071.
[23] H.M. Liu, W.S. Yang, Energy Environ. Sci. 4 (2011) 4000.
[24] B.D.H. Park, S.T. Lim, S.J. Hwang, C.S. Yoon, Y.K. Sun, J.H. Choy, Adv. Mater. 17 (2005) 2834.
[25] E. Hosono, T. Saito, J. Hoshino, Y. Mizuno, M. Okubo, D. Asakura, K. Kagesawa, D.N. Hamane, T. Kudo, H.S. Zhou, CrystEngComm 15 (2013) 2592.
[26] M.G. Kim, M. Jo, Y.S. Hong, J. Cho, Chem. Commun. 2 (2009) 218.
[27] H.W. Lee, P. Muralidharan, R. Ruffo, C.M. Mari, Y. Cui, D.K. Kim, Nano Lett. 10 (2010) 3852.
[28] S.J. Shi, Y.J. Mai, Y.Y. Tang, C.D. Gu, X.L. Wang, J.P. Tu, Electrochim. Acta 77 (2012) 39.
[29] Y.Q. Qiao, X.L. Wang, Y.J. Mai, J.Y. Xiang, D. Zhang, C.D. Gu, J.P. Tu, J. Power Sources 196 (2011) 8706.
[30] M.H. Lee, J.Y. Kim, H.K. Song, Chem. Commun. 46 (2010) 6795.
[31] C.F. Yang, J.J. Huang, L.G. Huang, G.J. Wang, J. Power Sources 226 (2013) 219.
[32] Y. Jiang, Z. Yang, W. Luo, X.L. Hu, Y.H. Huang, Phys. Chem. Chem. Phys. 15 (2013) 2954.
[33] L.J. Xi, C.W. Cao, R.G. Ma, Y. Wang, S.L. Yang, J.Q. Deng, M. Gao, F. Lian, Z.G. Lu, C.Y. Chung, Phys. Chem. Chem. Phys. 15 (2013) 16579.
[34] J.Z. Kong, H.F. Zhai, C. Ren, M.Y. Gao, X. Zhang, H. Li, J.X. Li, Z. Tang, F. Zhou, J. Alloys Compd. 577 (2013) 507.
[35] L.G. Xue, Z.H. Fu, Y. Yao, T. Huang, A.S. Yu, Electrochim. Acta 55 (2010) 7310.
[36] Q. Jiang, Y.L. Xu, C.J. Zhao, X.Z. Qian, S.W. Zheng, J. Solid State Electrochem. 16 (2012) 1503.
[37] K.C. Jiang, S. Xin, J.S. Lee, J. Kim, X.L. Xiao, Y.G. Guo, Phys. Chem. Chem. Phys. 14 (2012) 2934.
[38] H.X. Ji, L.L. Zhang, M.T. Pettes, H.F. Li, S.S. Chen, L. Shi, R. Piner, R.S. Ruoff, Nano Lett. 12 (2012) 2446.
[39] L. Zhou, H.B. Wu, T. Zhua, X.W. Lou, J. Mater. Chem. 22 (2012) 827.
[40] J. Li, H.C. Zeng, J. Am. Chem. Soc. 129 (2007) 15839.
[41] Z.J. Du, S.C. Zhang, Y. Liu, J.F. Zhao, R.X. Lin, T. Jiang, J. Mater. Chem. 22 (2012) 11636.
[42] L. He, S.C. Zhang, X. Wei, Z.J. Du, G.R. Liu, Y.L. Xing, J. Power Sources 220 (2012) 228.
[43] Y.L. Ding, X.B. Zhao, J. Xie, G.S. Cao, T.J. Zhu, H.M. Yu, C.Y. Sun, J. Mater. Chem. 21 (2011) 9475.
[44] J.Y. Luo, L. Cheng, Y.Y. Xia, Electrochem. Commun. 9 (2007) 1404.
[45] L. Zhou, D.Y. Zhao, X.W. Lou, Adv. Mater. 24 (2012) 745.
[46] J.F. Li, S.L. Xiong, X.W. Lia, Y.T. Qian, Nanoscale 5 (2013) 2045.
[47] J.W. Lang, L.B. Kong, W.J. Wu, Y.C. Luo, L. Kang, Chem. Commun. 35 (2008) 4213.
[48] Y.Q. Zhang, X.H. Xia, J.P. Tu, Y.J. Mai, S.J. Shi, X.L. Wang, C.D. Gu, J. Power Sources 199 (2012) 413.
[49] S.H. Kang, M.M. Thackeray, C.S. Johnson, J.T. Vaughey, S.A. Hackney, Electrochem. Commun. 8 (2006) 1531.
[50] J.S. Kim, C.S. Johnson, J.T. Vaughey, M.M. Thackeray, S.A. Hackney, W. Yoon, C.P. Grey, Chem. Mater. 16 (2004) 1996.
[51] W.S. Yoon, S. Iannopollo, C.P. Grey, D. Carlier, J. Gorman, J. Reed, G. Ceder, Electrochem. Solid State Lett. 7 (2004) A167.
[52] M.M. Thackeray, S.H. Kang, C.S. Johnson, J.T. Vaughey, R. Benedek, S.A. Hackney, J. Mater. Chem. 17 (2007) 3112.
[53] C.S. Johnson, N. Li, C. Lefief, J.T. Vaughey, M.M. Thackeray, Chem. Mater. 20 (2008) 6095.
[54] A. Ito, D. Li, Y. Sato, M. Arao, M. Watanabe, M. Hatano, H. Horie, Y. Ohsaw, J. Power Sources 195 (2010) 567.
[55] J. Park, J.H. Seo, G. Plett, W. Lu, A.M. Sastry, Electrochem. Solid State Lett. 14 (2011) A14.
[56] D.H. Jang, Y.J. Shin, S.M. Oh, J. Electrochem. Soc. 143 (1996) 2204.
[57] M. Wohlfahrt-Mehrens, C. Vogler, J. Garche, J. Power Sources 127 (2004) 58.
[58] I. Bloom, L. Trahey, A. Abouimrane, I. Belharouak, X.F. Zhang, Q.L. Wu, W.Q. Lu, D.P. Abraham, M. Bettge, J.W. Elam, X.B. Meng, A.K. Burrell, C. Ban, R. Tenent, J. Nanda, N. Dudney, J. Power Sources 249 (2014) 509.
[59] S.K. Martha, J. Nanda, Y. Kim, R.R. Unocic, S. Pannala, N.J. Dudney, J. Mater. Chem. A 1 (2013) 5587.
[60] H.L. Hayley, Y. Naoaki, S.M. Ying, K. Sundeep, B. Julien, P.G. Clare, S.-H. Yang, Chem. Mater. 19 (2007) 2551.
[61] J. Liu, Q.Y. Wang, B. Reeja-Jayan, A. Manthiram, Electrochem. Commun. 12 (2010) 750.
[62] S.K. Hu, G.H. Cheng, M.Y. Cheng, B.J. Hwang, R. Santhanam, J. Power Sources 188 (2009) 564.